FCS cell surface measurements—Photophysical limitations and consequences on molecular ensembles with heterogenic mobilities

ARTICLE *in* CYTOMETRY PART A · DECEMBER 2005

Impact Factor: 2.93 · DOI: 10.1002/cyto.a.20193 · Source: PubMed

2 AUTHORS:

Jerker Widengren
KTH Royal Institute of Technology
108 PUBLICATIONS **3,967** CITATIONS
SEE PROFILE

Per Thyberg
KTH Royal Institute of Technology
28 PUBLICATIONS **568** CITATIONS
SEE PROFILE

 Cytometry Part A 68A:101–112 (2005)

FCS Cell Surface Measurements—Photophysical Limitations and Consequences on Molecular Ensembles with Heterogenic Mobilities

Jerker Widengren* and Per Thyberg

Department of Physics, Division of Experimental Biomolecular Physics, Royal Institute of Technology, Albanova University Center, 106 91 Stockholm, Sweden

Received 16 December 2004; Revision Received 4 July 2005; Accepted 9 August 2005

Background: Fluorescence Correlation Spectroscopy is a powerful method to analyze densities and diffusive behavior of molecules in membranes, but effects of photodegradation can easily be overlooked.

Method: Based on experimental photophysical parameters, calculations were performed to analyze the consequences of photobleaching in fluorescence correlation spectroscopy (FCS) cell surface experiments, covering a range of standard measurement conditions.

Results: Cumulative effects of photobleaching can be prominent, although an absolute majority of the fluorescent molecules would pass the laser excitation beam without being photobleached. Given a distribution of molecules on a cell surface with different diffusive properties, the fraction of molecules that is actually analyzed depends strongly on the excitation intensities and measurement times, as well as on the size of the reservoir of freely diffusing molecules. Both the slower and the faster diffusing molecules can be disfavored.

Conclusions: Apart from quantifying photobleaching effects, the calculations suggest that the effects can be used to extract additional information, for instance about the size of the reservoirs of free diffusion. By certain choices of measurement conditions, it may be possible to more specifically analyze certain species within a population, based on their different diffusive properties, different areas of free diffusion, or different kinetics of possible transient binding. © 2005 International Society for Analytical Cytology

Key terms: fluorescence correlation spectroscopy; photobleaching; diffusion; cell membrane

Photophysical and photochemical aspects of dyes are of great importance for all applications of fluorescence spectroscopy where a high read-out rate or a high sensitivity is required. In FCS, fluorescence intensity fluctuations are studied, brought about by thermodynamic fluctuations among sparse numbers of molecules (1–3). The fluctuation behavior can in principle provide information about any molecular dynamic process, from the nanosecond to millisecond time range, that is reflected as a change in the detected fluorescence intensity. This has made FCS as a useful tool to study a wide range of phenomena (see (4–8) for reviews). A major figure-of-merit in FCS measurements is the detected fluorescence rate per molecule, F_M (9,10). A successful strategy to improve F_M is to use a small open confocal detection volume (fractions of a femtoliter) (11,12). This facilitates a fast exchange of fluorescently marked molecules by diffusion through the volume. Thereby, higher excitation intensities can be applied without photobleaching the molecules, thus providing higher fluorescence emission rates per molecule. It also lowers the background due to Raman scattering, since at constant excitation intensities, the detected Raman scattering is proportional to the detection volume. Although a minimized detection volume is a successful concept for highly mobile molecules, photobleaching can still be a problem for slowly moving fluorescent molecules. Application of excitation intensities close to saturation, feasible for FCS measurements of highly mobile molecules, then typically results in significant fractions of the molecules being photobleached while passing the excitation volume (13,14). This results in apparently shorter transit times as judged from the FCS curves. By a successive reduction in the excitation intensity, the absence of this effect can be taken as an indication that most molecules pass the detection volume without being photobleached.

The development of the FCS technique over the last decade has opened for applications in cell biology to monitor densities, mobilities, and kinetics of very small numbers of molecules, over wide ranges of rates, and in small regions of cells (see (15) for a review). In cellular

Contract grant sponsors: The Swedish Medical Research Council, the Swedish Cancer Foundation, Åke Wibergs Stiftelse, Magnus Bergwalls Stiftelse, and the Swedish Medical Society.

*Correspondence to: Jerker Widengren.
E-mail: jerker@biomolphysics.kth.se

Published online 19 October 2005 in Wiley InterScience (www.interscience.wiley.com).
DOI: 10.1002/cyto.a.20193

membranes, the understanding of the mobility of proteins is essential for elucidating the mechanisms and kinetics of many membrane-associated functions (16). The ability of FCS, along with other ultrasensitive fluorescence spectroscopic approaches, to visualize and monitor protein dynamics and biological processes, thus, has the potential to revolutionize many areas in the biomedical field (see (17) for a review). Because of this, the FCS technique has over the last few years found a strongly increased use for characterization of molecules on cell surfaces and inside cells (18–36). Compared with FCS studies in aqueous solutions, FCS cell studies are associated with additional features and complications, for which treatments have been suggested. Such features and complications include anomalous diffusion (25,37), limited volumes of diffusion (38,39), unspecific probe interactions with cellular structures (40), autofluorescence (20), fluctuations and topography effects of the membrane itself (41–43), and diffusion biases due to weak optical trapping of the fluorescent molecules under study (44).

For cellular studies with FCS, photobleaching is a major limitation, aggravated by the finite number of molecules that are free to diffuse in and out of the volume of detection. This limited reservoir of molecules reduces the replenishment of fluorescently viable molecules into the detection volume, enhancing the degree of depletion of the fluorescent molecules. This has been pointed out by several investigators (13,20,24). Moreover, Delon et al. have studied the relation between mobility, photobleaching, and compartmentalization in constrained, three-dimensional compartments (45). Still, the effects tend to be overlooked or underestimated in many cellular studies based on FCS.

In this study, we investigated more in detail effects of photobleaching under conditions typical for FCS studies on cellular membranes, in which studies, the investigated molecules are confined to a two-dimensional area of finite size. The purpose was to identify proper measurement conditions where the effects are minimized, as well as to indicate how the effects can be used to extract additional information about the diffusive behavior of the investigated molecules. First, the photophysical properties of tetramethyl-rhodamine isothiocyanate (TMR) in aqueous solution and of TMR-epidermal growth factor (TMR-EGF) bound to EGF receptors on the surfaces of rat bladder carcinoma cells were measured by FCS. On the basis of these properties, the effects of photobleaching were calculated for an idealized cell surface model with parameters representative for a typical FCS measurement. As compared with real measurements, calculations that simulate measurements make it possible to focus on pure photodepletion effects, and to exclude the influence of a range of features and parameters inherent with the heterogeneity and complexity of a living cell.

MATERIALS AND METHODS

Experimental

The main experimental setup has been described earlier (12,46). In brief, the beam of an argon ion laser (Spectra Physics Model 165, Mount.View, CA) operated at 514.5 nm was fed into an epi-illuminated confocal microscope [dichroic mirror (Leitz TK580, Wetzlar, Germany), water immersion objective (Zeiss Plan-Neofluar 63× NA 1.2, Jena, Germany), pinhole (30 μm in diameter), fluorescence band-pass filter (Omega Optics 585DF45, Brattleboro, VT)]. The excitation power was regulated from the power supply of the laser and by neutral OD filters (Schott, Jena, Germany) and measured by a silicon photodiode (Graseby Optronics, Orlando, FL) under the microscope objective. The fluorescence light was detected by two avalanche photodiodes (EG&G model SPCM-100, Vaudreuil, Canada), whose pulses were passed to a PC-based correlator (ALV model 5000, Langen, Germany). The detection volume was defined by the dimensions of the laser beam focus and the collection efficiency function of the confocal setup. The laser beam $1/e^2$-radius in the detection plane, ω_0 was 0.3 μm ± 10%.

TMR (Molecular probes, Eugene, OR) was measured in a hanging droplet of aqueous solution placed under the microscope objective. TMR-labelled EGF (TMR-EGF) (Molecular probes) was added into the buffer (PBS) of a Petri dish in which cells from a rat bladder carcinoma cell line had been grown. After a few min of incubation at room temperature, FCS measurements were performed. By scanning vertically one could distinguish the freely diffusing EGF molecules from those bound to the cell surface.

Theory and Calculation Approach

To estimate effects of photobleaching in cell surface FCS measurements, calculations were performed, where the concentration (surface density) of fluorescently marked molecules as a function of space and time, $c(\bar{r},t)$, was calculated within a circular disc of radius R_{cell}. The circular disc represents the cell surface, $\bar{r}$ is the location within the disc, and t denotes the time after onset of the excitation, located in the center of the disc ($\bar{r}$ = (0,0)). The fluorescent molecules undergo translational diffusion within the circular disc, and photobleaching takes place in the disc center as an effect of excitation. The spatio–temporal dependence of $c(\bar{r},t)$ is then given by the two-dimensional diffusion equation with a negative source term:

$$\frac{dc(\bar{r},t)}{dt} = D\nabla^2 c(\bar{r},t) - k_D(\bar{r})\ c(\bar{r},t) \qquad (1)$$

Because of the radial symmetry, $\bar{c}(\bar{r},t)$ can be calculated as a function of the radial distance from the center of the disc, $r = |\bar{r}|$. In cylindrical coordinates, (r,φ), Eq. (1) then takes the form

$$\frac{dc(r,t)}{dt} = D\left[\frac{d^2}{dr^2}c(r,t) + \frac{1}{r}\frac{d}{dr}\ c(r,t)\right] - k_D(r)\ c(r,t) \qquad (2)$$

As an initial condition to Eq. (2), at the onset of excitation in the center of the disc ($t = 0$)

$$c(0,r) = c_0\ \forall r \qquad (3)$$

where the initial concentration, c_0, hereafter is normalized to unity. $c(r,t)$ then corresponds to the fraction of fluorescent molecules, located in (r,t) in the spatio–temporal domain that has survived photobleaching. Because of the radial symmetry and since no concentration gradient can exist at the physical borders of the disc, we can apply as a boundary condition:

$$\frac{dc(r,t)}{dr} = 0 \quad \text{for } r = 0 \text{ and } r = R_{\text{cell}} \tag{4}$$

The rate of degradation, $k_D(r)$, is assumed to be proportional to the fraction of fluorescent molecules that are in their excited singlet states:

$$k_D(r) = k_{10}\,\Phi_D\,S_1(r) \tag{5}$$

where k_{10} is the deexcitation rate of excited singlet state (S_1) to the ground singlet state (S_0), and Φ_D is the photodestruction quantum yield, defined as the probability that photobleaching takes place following excitation from S_0 to S_1. $S_1(r)$ denotes the steady-state population probability of the excited singlet state of TMR.

Based on a three state model, including S_0, S_1, and the lowest triplet state T, and with the population of S_0 and S_1, and T normalized to $S_0(r) + S_1(r) + T(r) = 1$, $S_1(r)$ can be written:

$$S_1(r) = \frac{k_{\text{exc}}(r)\,k_T}{k_{\text{exc}}(r)\,(k_T + k_{\text{ISC}}) + k_{10}\,k_T} \tag{6}$$

Here, $k_{\text{exc}}(r)$ is the rate of excitation of S_0 to S_1, k_{ISC} is the rate of intersystem crossing from S_1 to T, and k_T denotes the deactivation rate of T to S_0. $k_{\text{exc}}(r)$ is proportional to the excitation intensity of the laser at the cell surface, which is assumed to be Gaussian distributed:

$$k_{\text{exc}}(r) = \sigma I(r) = \sigma I_0 e^{-[2r^2/\omega_0{}^2]} \tag{7}$$

Here, ω_0 denotes the radial distance from the center of the laser beam focus at which the excitation intensity, $I(r)$, has dropped to $1/e^2$ of its central peak value, $I_0 = I(0)$, and σ denotes the excitation cross section of the fluorophores.

To quantify the relative decrease of the number of molecules that are detected within the detection volume following the onset of excitation at $t = 0$, we introduce the normalized number of detected molecules as

$$\bar{N}(t) = \frac{N(t)}{N_0} = \frac{\int_{r=0}^{R_{\text{cell}}} \text{CEF}(r)\,c(r,t)\,S_1(r) \times 2\pi r\,dr}{\int_{r=0}^{R_{\text{cell}}} \text{CEF}(r)\,c(r,0)\,S_1(r) \times 2\pi r\,dr} = \frac{\int_{r=0}^{R_{\text{cell}}} \text{CEF}(r)\,c(r,t)\,S_1(r) \times r\,dr}{\int_{r=0}^{R_{\text{cell}}} \text{CEF}(r)\,S_1(r)\,r\,dr} \tag{8}$$

Here, CEF(r) is the collection efficiency function of the confocal system, determined by the laser beam dimensions, the magnification and numerical aperture of the objective, and the pinhole diameter in the image plane (12). $c(r,0) = c_0$ is set to unity (Eq. (3)).

A numerical approach based on the Crank-Nicholsson algorithm (47) was applied so as to calculate $c(r,t)$ according to Eq. (2) and its boundary and initial conditions. $c(r,t)$ was then approximated on a discrete form, and calculated as a discrete array c_{ij}, where $r = i\,dr$ and $t = j\,dt$. For each calculation, the spatio–temporal distribution of $c(r,t)$ was calculated for 1,000 × 10,000 data points, 1,000 steps along the full radial distance of the calculated cell, R_{cell}, and 10,000 steps along the time axis (see appendix).

RESULTS AND DISCUSSION

FCS Experiments Determining TMR Photophysical Parameters

The photodynamic properties of TMR were determined in aqueous solution. FCS measurements were performed at excitation powers ranging from 0.2 to 4 mW (corresponding to mean excitation intensities from 0.07 to 1.5 MW/cm^2). For molecules measured by FCS that undergo translational diffusion and singlet–triplet transitions, the measured FCS curves can be described by (46)

$$G_T(\tau) = \frac{1}{N(1-\bar{T})}\left(\frac{1}{1+4D\tau/\omega_1{}^2}\right)\left(\frac{1}{1+4D\,\tau/\omega_2{}^2}\right)^{1/2} \times [1 - \bar{T} + \bar{T}\,\exp(-\tau/\tau_T)] + 1 \tag{9}$$

Here, $\bar{T} = \bar{S}_1\,k_{\text{ISC}}/k_T$ is the mean of $T(r)$ within the detection volume and $\tau_T = 1/[(\bar{S}_1/(\bar{S}_1 + \bar{S}_0))\,k_{\text{ISC}} + k_T]$ is the relaxation time of the singlet–triplet transitions. $\bar{S}_0$ and $\bar{S}_1$ signify the means of $S_0(r)$ and $S_1(r)$ within the detection volume, and ω_1 and ω_2 denote the $1/e^2$ extensions of the detection volume in the radial direction and along the beam axis, respectively.

k_{ISC} and k_T were determined in a global fit from an overdetermined set of equations, given the $\bar{T}$ and τ_T of nine correlation curves measured over the whole range of excitation intensities (46). This analysis yielded $k_{\text{ISC}} = 1.0 \times 10^6\ \text{s}^{-1}$ and $k_T = 0.6 \times 10^6\ \text{s}^{-1}$, respectively. The excitation cross section, σ, of TMR at 515 nm was estimated to 1.1×10^{-16} cm^2, with k_{10} fixed to $435 \times 10^6\ \text{s}^{-1}$ (48).

FCS measurements were performed on surfaces of cells from a rat bladder carcinoma cell line after a few min of incubation with TMR-EGF and subsequent rinsing with PBS buffer. Binding was observed in a similar fashion as reported in (31). The excitation powers ranged from 10 to 550 μW (corresponding to mean excitation intensities of ~3.5–200 kW/cm^2). For the lowest range of excitation intensities, the measured translational diffusion time, $\tau_D = \omega_1{}^2/4D$, was of the order 20 ms and did not change significantly with variation of excitation intensities. With the assumption that only a minor fraction of the labeled molecules passing the detection volume are bleached in this excitation intensity range, the diffusion coefficient, D, of the measured molecules could be estimated to 7×10^{-9} cm^2/s. This is an order of magnitude faster diffusion than that reported from fluorescence recovery after photobleaching (FRAP) measurements (49). Possible reasons for this difference are discussed later. With higher excitation intensities, the overall decay of the correlation

curves was increasingly faster. This increased decay can be attributed to photobleaching, and the measured correlation curves can be modelled as (13,14).

$$G_{BT}(\tau) = [G_T(\tau) - 1] \times \lfloor 1 - B + B\ \exp(-k_{Dexp}\ \tau) \rfloor + 1 \quad (10)$$

For excitation intensities above 100 kW/cm^2, the additional exponential decay in the correlation curves could be noticed to have a relative amplitude, B, of ~0.6–0.7. The relaxation rate, k_{Dexp}, of this exponential decay scaled with the excitation intensity. From the measured parameters of B and k_{Dexp}, the photodestruction quantum yield, Φ_D, was estimated to be 4×10^{-6} by use of (13)

$$\Phi_D = \frac{B k_{Dexp}}{\bar{S}_1 (k_{10} + k_{ISC})} \quad (11)$$

The measured Φ_D is somewhat higher than what has previously been reported (50) for TMR-labelled lipids in an artificial membrane ($\Phi_D = 2 \times 10^{-6}$). Possible reasons for this discrepancy are discussed in the next section.

Calculations of $c(r,t)$ after Onset of Excitation

On the basis of Eqs. (2)–(4), using a Crank-Nicholsson approach, the dependence of $c(r,t)$ on excitation intensity, the size of the cell or domain within which the molecules are free to diffuse, the measurement time, and the diffusive speed was investigated. In the calculations, the following photophysical parameters determined earlier for TMR was used: $k_{ISC} = 1.0 \times 10^6\ s^{-1}$, $k_T = 0.6 \times 10^6\ s^{-1}$, and $\sigma = 1.1 \times 10^{-16}$ cm^2. For Φ_D, the literature value (50) of 2×10^{-6} was used, instead of that determined from our FCS measurements. The beam radius ω_0 was set to 0.3 μm, and k_{10} to $435 \times 10^6\ s^{-1}$ (48). The collection efficiency function, CEF(r), was calculated as described in (46), and yielded together with $k_{exc}(r)$ of Eq. (7) a $1/e^2$ radial extension of the detection volume of $\omega_1 = 0.23$ μm.

For clarity, it should be pointed out that the singlet–triplet state properties determined for free TMR in aqueous solution are probably somewhat different from those of TMR-EGF in cell membranes (different microenvironments in terms of viscosity, oxygen concentrations, etc.). Moreover, the photobleaching quantum yield was determined for TMR-EGF in the cellular membranes, but at higher excitation intensities than those used in the calculations. For many dyes, Φ_D increases at excitation intensities approaching saturation (13,14). Apart from irreversible photobleaching, photo-induced reversible states of the fluorophores can also reduce the correlation times (51). This could explain why we obtained a higherΦ_D than in (50), and motivates the use of their value in the calculations. However, in the following calculations, the purpose was not to predict the consequences for a particular fluorescently marked molecule (TMR-EGF), but to investigate principal effects of photobleaching. With the fluorophore parameter values used, the calculations are adequate and representative for a wide range of commonly used fluorophores.

Photobleaching Depletion Profiles Versus Diffusive Speed, Excitation Power, and Measurement Time

Figures 1a–1d show the calculated radial profiles of $c(r,t)$ for molecules with different diffusion coefficients, within a cell with a radius of $R_{cell} = 5$ μm, after a measurement time of 60 s (typical duration of a FCS measurement) for different excitation powers ranging from 2.5 to 250 μW. Experimentally, from the performed FCS measurements at excitation powers in the lowest part of this range, no effect of photobleaching can be noticed from the shape of the correlation curves. The probability of photobleaching can thus be assumed to be very small for a single transit of a molecule through the area of excitation. In agreement with this, given the photophysical and measurement parameters above, with $D = 7 \times 10^{-9}$ cm^2/s, and for an excitation power of 2.5 μW, photobleaching can be expected to occur in less than one percent of the molecular transits. Nonetheless, the calculations show that the accumulated depletion of molecules can still be significant also at lower excitation powers. Clearly, the fact that the excitation intensity is set at a level far below that at which photobleaching can be noticed from the shape of the correlation curves does not guarantee that effects of photobleaching can be neglected.

Comparing the set of concentration profiles in the Figures 1a–1d, one can note that the depletion is mainly local for slowly diffusing species, while an increasingly predominant overall depletion takes place with faster diffusion of the fluorescent species. In the presence of a distribution of fluorescent species on the surface having different diffusion properties, one would therefore expect preferentially the fraction of fast diffusing fluorescent molecules to remain more intact in the area of detection (radial distance <0.3 μm). Because of this D-dependent depletion, a situation would easily emerge, where fast diffusing species are detected and analyzed to a larger extent than their slower counterparts. For low diffusion coefficients, in particular below 10^{-10} cm^2/s, the local depletion of fluorescent molecules is very prominent, also for the lower range of excitation intensities calculated. The presence of a slowly diffusing fraction of molecules on a cell surface can therefore not be expected to be clearly detectable as an increase in the average measured diffusion time following a reduction of excitation intensity. This D-dependent selection provides a possible explanation why the diffusion coefficient of TMR-EGF measured by FCS was about an order of magnitude faster than that measured by FRAP (see FCS Experiments Determining TMR Photophysical Parameters section). However, the different approaches of the methods can also contribute to this discrepancy. In FCS, the diffusive properties within the excitation volume is measured, while FRAP measures the replenishment of fluorescent molecules by diffusion following a total depletion of fluorescence in the detection volume by a strong laser beam. Consequently, FRAP averages the diffusive properties of a larger region, the one from which molecules enter the detection volume during concentration recovery.

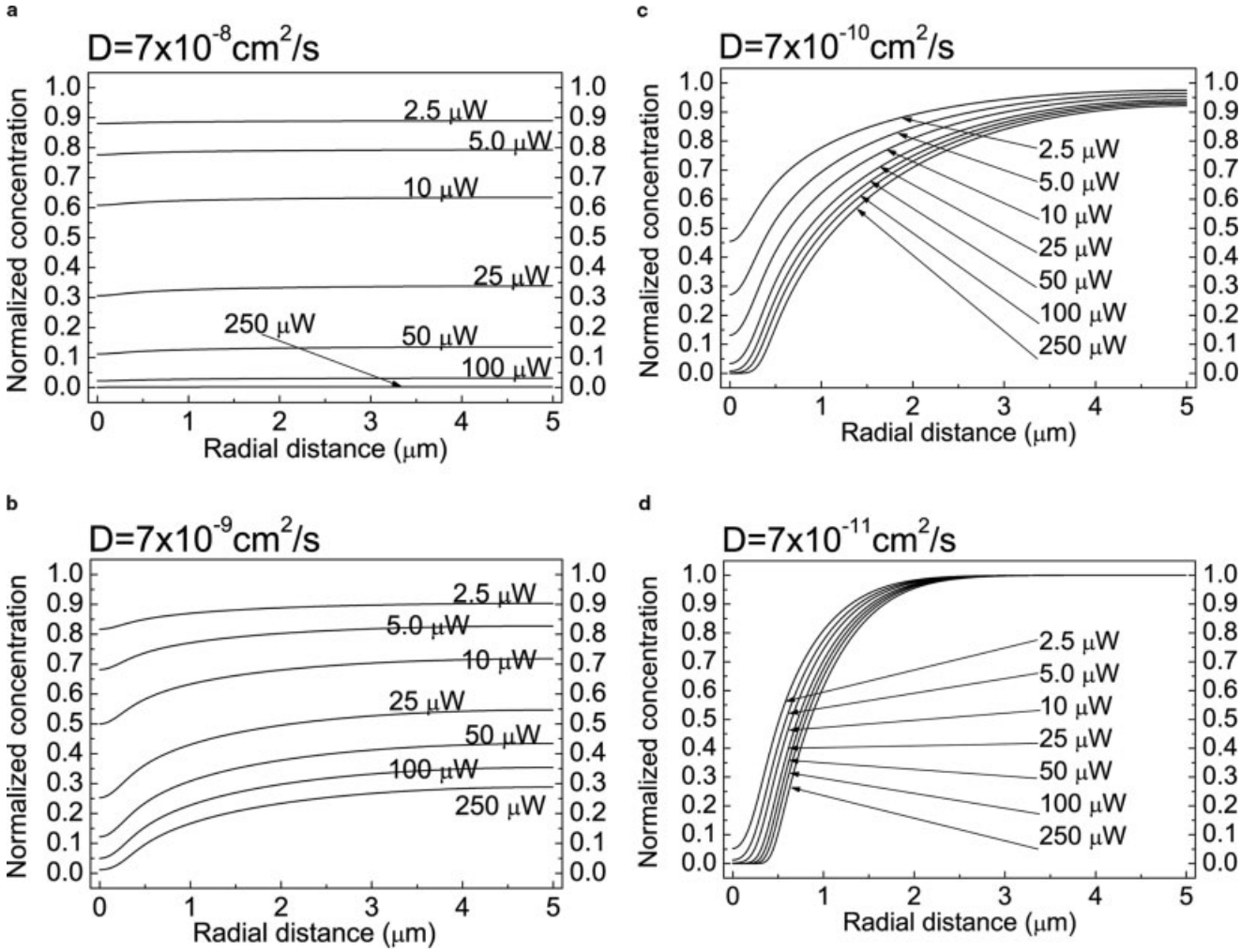

FIG. 1. Calculated radial profiles of $c(r,t)$, corresponding to the fraction of fluorescent molecules that has survived photobleaching, after a measurement/exposure time of 60 s, and for different excitation powers ranging from 2.5 to 250 μW. $R_{cell} = 5$ μm. (**a**) $D = 7 \times 10^{-8}$ cm^2/s (**b**) $D = 7 \times 10^{-9}$ cm^2/s (**c**) $D = 7 \times 10^{-10}$ cm^2/s, and (**d**) $D = 7 \times 10^{-11}$ cm^2/s.

Similar depletion patterns as in Figures 1a–1d can be seen in calculations performed to investigate effects of different measurement/exposure times (Figs. 2a–2d). It can be noted, especially for the slower species, that when a given excitation energy, ([excitation power] × [exposure time]), is distributed over a longer exposure time, the depletion becomes more global.

Photophysical Effects on the Amount of Fluorescence and Number of Molecules Detected in the Detection Volume

Because of diffusion-dependent differences in the spatio–temporal patterns of depletion (as exemplified in Figs. 1a–1d and 2a–2d), the actual distribution that is detected from a distribution of fluorescent species on the surface having different diffusion properties, will change during the course of a measurement, or with different excitation intensities applied. This is illustrated in Figure 3a, which shows the normalized concentration in the detection area (Eq. (8)) of remaining, still not photobleached, fluorescent species with different diffusive properties, plotted versus measurement time. A higher depletion of fast moving species can be noted for longer measurement times. This can be understood by considering the total bleaching rate in absolute terms, $k_{D\text{tot}}(t)$, which can be expressed as the negative source term in Eq. (2), integrated over the excitation volume:

$$k_{D\text{tot}}(t) = \int_{r=0}^{R_{cell}} k_D(r)\, c(r,t)\, 2\pi r\, dr \qquad (12)$$

$k_{D\text{tot}}(t)$ will initially be higher for fast diffusing species, since $c(r,t)$ will not be locally depleted to the same extent as for the slower species. However, the whole reservoir of molecules within the cell surface will then be emptied by

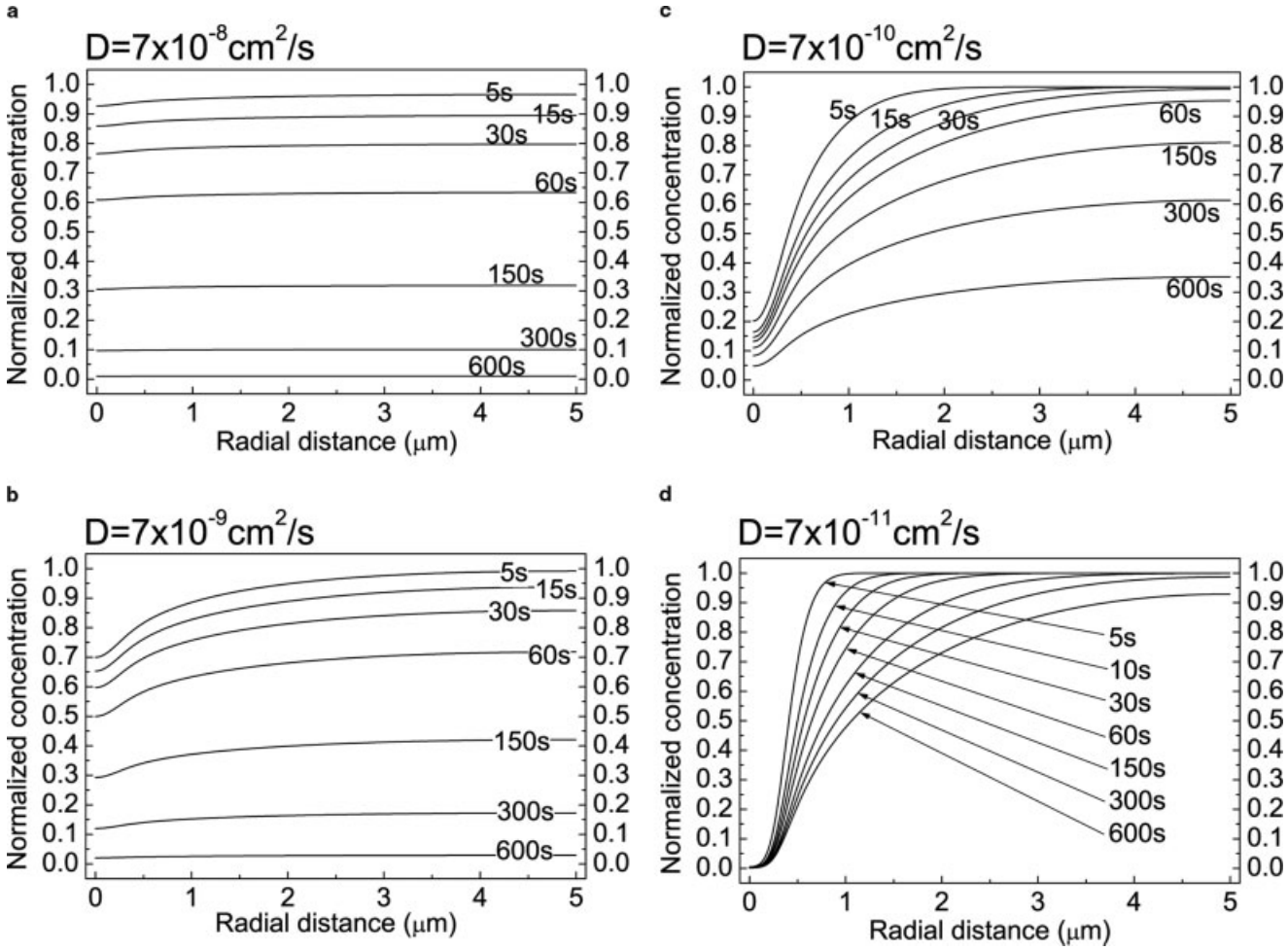

FIG. 2. Radial profiles of $c(r,t)$. R_{cell} = 5 μm. Measurement/exposure times ranging from 5 to 600 s. Excitation power of the laser 10 μW. (**a**) $D = 7 \times 10^{-8}$ cm^2/s (**b**) $D = 7 \times 10^{-9}$ cm^2/s (**c**) $D = 7 \times 10^{-10}$ cm^2/s, and (**d**) $D = 7 \times 10^{-11}$ cm^2/s.

a higher rate than for the slow molecules, leading also to a higher accumulated depletion at exposure time t, given by

$$K_{D\text{tot}}(t) = \int_{t=0}^{t} k_{D\text{tot}}(t)\, dt \qquad (13)$$

A population of fast and slow molecules present in equal densities will initially be measured as predominantly fast molecules, due to a close to instantaneous (sec) local depletion of the slow molecules caused by photobleaching. However, with longer exposure/measurement times t, a stronger global depletion due to a higher $k_{D\text{tot}}(t)$ of the fast species will result in an inverse situation. What fraction of molecules that will dominate the detected population, and when, depends on a combination of diffusive speed, measuring time, total area of the cell reservoir, and excitation power, where long measurement times and small reservoirs in general favour the slower fraction(s) of the molecules.

In Figure 3b, it is illustrated how these effects can influence the actually measured autocorrelation curves. The curves are calculated from Eq. (9) (triplet state fluctuations are not considered), for a mixture of two species present in equal amounts, with equal fluorescence brigthnesses, and with diffusion coefficients $D = 7 \times 10^{-9}$ and 7×10^{-10} cm^2/s, respectively. The calculations are based on the parameters used in Figure 3a, and the $\bar{N}(t)$ for each of the species at three different exposure times (0, 30, and 600 s), and by replacing N with the product $N \times \bar{N}(t)$ for each of the species in Eq. (9). Considerable distortions both with respect to amplitude (1/N, see inset), decay time, and shape can be generated in FCS curves originating from differences in the spatio–temporal patterns of photodepletion of the different species present.

In Figure 3c, the amount of fluorescence detected in the detection volume is plotted versus excitation power for fluorescence species assumed to be completely photostable and not limited by saturation (k_f), limited by singlet saturation only (k_{fs}), or limited by both singlet and triplet state saturation (k_{fst}). The amount of fluorescence detected for these species is compared with that estimated for species that undergo photobleaching with a photodes-

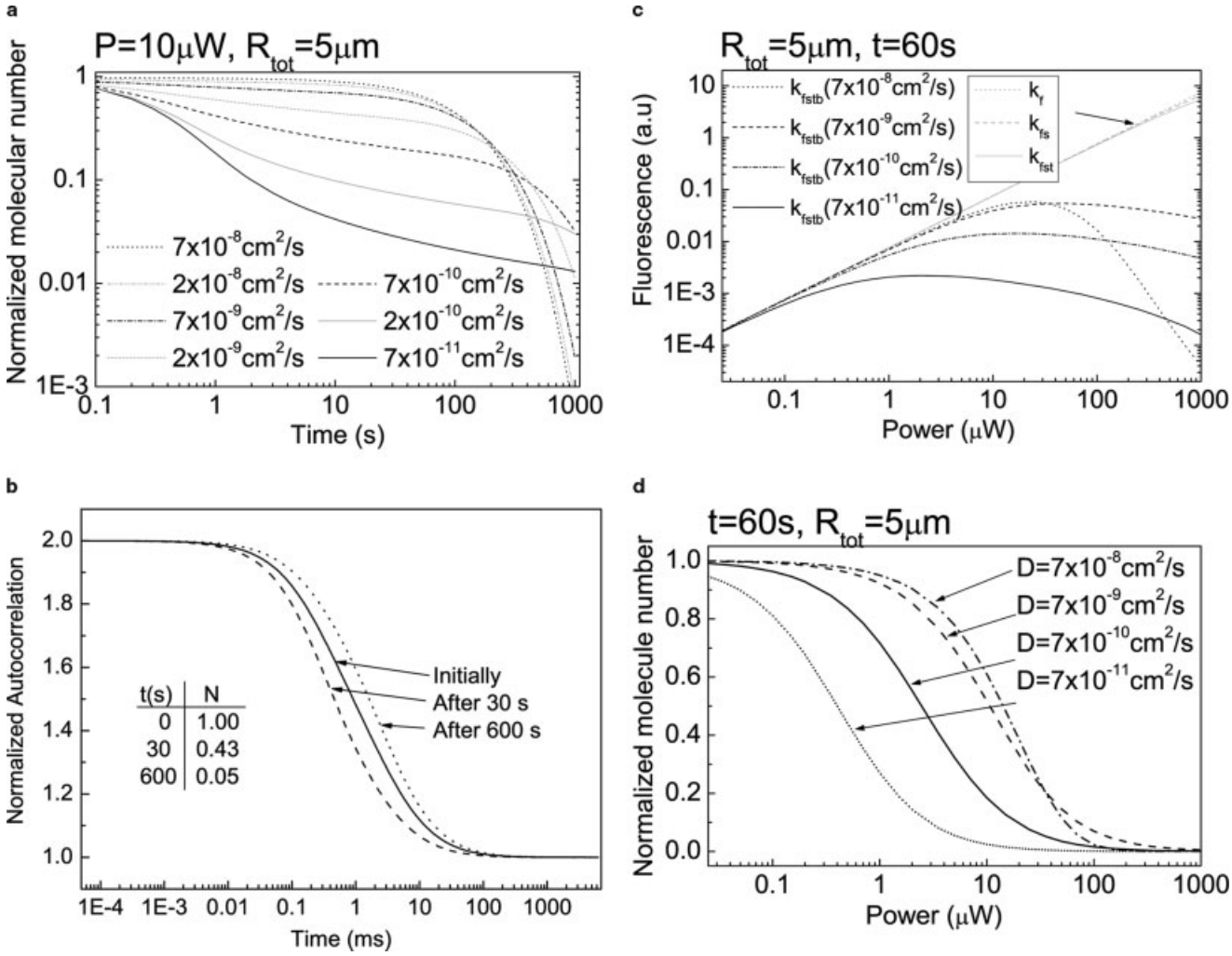

FIG. 3. (**a**) Mean fraction of molecules in the detection volume that has survived photobleaching ($\bar{N}(t)$ given by Eq. (8)) versus measurement/exposure time. The detection volume was calculated from the profile of the excitation (Eq. (7)), with $\omega_0 = 0.3$ μm, and the collection efficiency function, CEF (r), calculated as in (46), with a 63×, 1.2 N.A. objective and a pinhole with a diameter of 30 μm. $R_{cell} = 5$ μm, $P = 10$ μW. (**b**) Normalized FCS curves calculated from Eq. (9) for two species and with $\bar{T} = 0$. The two species are present in equal concentrations, with $D = 7 \times 10^{-9}$ and 7×10^{-10} cm^2/s, respectively. $P = 10$ μW, $R_{tot} = 5$ μm. The relative contributions to the correlation curves from each species is based on the calculated $\bar{N}(t)$ (see Figure 3a) at $t = 0$, 30, and 600 s, respectively. (**c**) Amount of fluorescence (arbitrary units) from the detection volume ($F(t)$, Eq. (14)) versus excitation power after 60 s measurement/exposure time. $R_{cell} = 5$ μm. $F(t)$ is calculated for species assumed to be completely photostable and not limited by saturation (k_f), limited by singlet saturation only (k_{fs}), or limited by both singlet and triplet state saturation (k_{fst}). The amount of fluorescence detected for these species is compared with that estimated for species that undergo photobleaching with a Φ_D of TMR (k_{fstb}). (**d**) Normalized number of fluorescent molecules in the detection area, $\bar{N}(t)$, versus excitation power for species with different diffusion constants. $R_{cell} = 5$ μm, measurement/exposure time = 60 s.

truction quantum yield of TMR (k_{fstb}). For k_f, k_{fs}, k_{fst}, and k_{fstb}, the total amount of detected fluorescence was calculated as:

$$F(t) = \int_0^{R_{cell}} \mathrm{CEF}(r)\, F(r)\, c(r,t)\, \Phi_F\, \Phi_{Fd}\, 2\pi r\, dr \qquad (14)$$

where $F(r) = k_{exc}(r)$, $k_{10}k_{exc}(r)/(k_{exc}(r)+k_{10})$, $k_{10}S_1(r)$, and $k_{10}S_1(r)$ for k_f, k_{fs},k_{fst}, and k_{fstb}, respectively. $c(r,t)$ is equal to unity for k_f, k_{fs}, and k_{fst} (no photobleaching), and is determined by Eqs. (2)–(4) for k_{fstb}. Φ_F denotes the fluorescence quantum yield (set to 0.3 (51)) and Φ_{Fd} signifies the overall quantum yield of fluorescence detection of the setup (estimated to 0.02). From the plots in Figure 3c, it can be noted that no matter if diffusion is slow or fast, the depletion due to photobleaching can be expected to be the main source of reduction of fluorescence in FCS cell surface studies. Effects of fluorescence saturation and triplet state population, which constitute major limitations to the detected fluorescence rate in FCS solution studies, play a very minor role.

In Figure 3d, the normalized concentration of fluorescent molecules in the detection area (Eq. (8)) is plotted versus measurement excitation power for species with different diffusive properties. These plots indicate where the upper limits of the excitation intensity are for species with

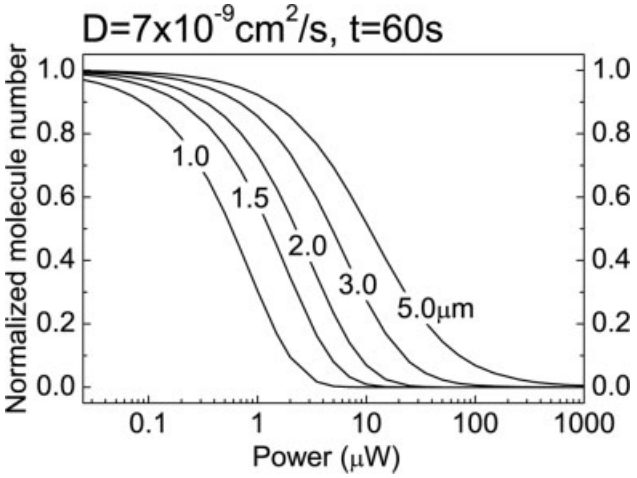

FIG. 4. Normalized number of fluorescent molecules in the detection area, $N(t)$, versus excitation power for different radii of the area within which the molecules are free to diffuse (R_{cell}). $D = 7 \times 10^{-9}$ cm^2/s, t = 60 s, P = 10 μW.

different diffusion properties. Above these limits, most of the initial concentration of fluorescent molecules in the detection volume is depleted by photobleaching. This can, if not considered, lead to a strong underestimation of the density of molecules at the cell surface.

Effects of the Size of the Reservoir Surface

On cells, molecules are rarely allowed to diffuse freely over their entire surfaces, but are often confined to sub-compartments or rafts within the cell membranes (52). It is therefore relevant to further consider how the size of the reservoir surface, within which the molecules can diffuse freely and from which replenishment of unbleached molecules can occur, can affect the outcome of a FCS measurement. In Figure 4, the calculated normalized number of detected molecules (Eq. (8)) after 60 s of measurement is plotted for a compound with $D = 7 \times 10^{-9}$ cm^2/s that is free to diffuse within an area of different R_{cell}. As expected, a reduction of R_{cell} can have a strong influence on the remaining fraction of unbleached molecules in the detection volume. Overall depletion effects due to confinement of the diffusion to a sub-compartment will be most pronounced for fast diffusing species.

Effects of Interconversion Between States with Different Diffusive Speeds

Proteins and other biomolecules embedded in or associated with cellular membranes can either diffuse freely, be immobilized or strongly retarded by association to scaffolds or aggregates, or be subject to active transport (53). They can also often be shown to interconvert between different diffusive behaviors. To investigate how this can influence the extent of photodepletion in FCS measurements, we considered a molecular species switching between two states with a fast (A) and a slow (B) diffusive behavior

$$\mathrm{A} \underset{k_{BA}}{\overset{k_{AB}}{\rightleftarrows}} \mathrm{B} \quad \text{with } D_A > D_B \tag{15}$$

Equation 1 can then be modified to

$$\begin{aligned}\frac{dc_A(\bar{r},t)}{dt} &= \left[D_A\nabla^2 c_A(\bar{r},t)\right] - \left[k_D(\bar{r}) \times c_A(\bar{r},t)\right] \\ &\quad - \left[k_{AB}c_A(\bar{r},t)\right] + \left[k_{BA}c_B(\bar{r},t)\right] \\ \frac{dc_B(\bar{r},t)}{dt} &= \left[D_B\nabla^2 c_B(\bar{r},t)\right] - \left[k_D(\bar{r}) \times c_B(\bar{r},t)\right] \\ &\quad + \left[k_{AB}c_A(\bar{r},t)\right] - \left[k_{BA}c_B(\bar{r},t)\right]\end{aligned} \tag{16}$$

with the initial condition in cylindrical coordinates $c_A(r,0) + c_B(r,0) = 1\ \forall r$, the boundary conditions of Eq. (4) valid for both $c_A(r,t)$ and $c_B(r,t)$, and with the sum of $c_A((r,t)$ and $c_B(r,t)$ replacing $c(r,t)$ in Eq. (8). In Figure 5, the calculated normalized concentration of a molecular species interconverting between two equally populated states, with $D_A = 7 \times 10^{-9}$ cm^2/s and $D_B = 7 \times 10^{-10}$ cm^2/s, respectively, is plotted versus r, and for different rates of interconversion. These examples illustrate that the rate of interconversion can strongly influence the spatio–temporal depletion patterns and $\bar{N}(t)$. Typically, three stages in $\bar{N}(t)$ can be identified (Figs. 5c and 5d). At start of exposure, local depletion of species B has a stronger effect on $\bar{N}(t)$ than that of $k_{Dtot}(t)$ (Eq. (13)) of species A. Then, the interconversion leads to a depletion profile, which is close to an average of those of A and B for slow interconversion rates, and approaches that of A for faster rates. At the next stage, $k_{Dtot}(t)$ of A starts to influence $\bar{N}(t)$ more strongly than the local depletion of B. The lower time limit when the cell can enter into this stage, t_{tr}, can be estimated from the relation between the rate of degradation $k_D(r)$ (Eq. (5)), integrated over the exposed area, and the total area of the cell, $t_{tr} = \pi R_{tot}^2/k_D(0)\pi\omega^2$. For P = 10 μW, this gives t_{tr} = 22 s and 139 s for R_{tot} = 2 μm (Fig. 5c) and 5 μm (Fig. 5d), respectively. In this, second stage, the interconverting species can in fact be more detectable, by a higher $\bar{N}(t)$, than both the A and B species alone. In the last stage, for long enough exposure times and/or small R_{tot}, the B state will dominate over the A state due to the high $k_{Dtot}(t)$ of A. The interconverting species will be less detectable than B, but more than A, and slowly interconverting species will be favoured, in terms of $\bar{N}(t)$, over fast interconverting species. The insets of Figs. 5c and 5d show the corresponding $\bar{N}(t)$ with $D_B = 7 \cdot 10^{-11}$ cm^2/s. Here, the second stage with the $\bar{N}(t)$ of interconverting species dominating over $\bar{N}(t)$ of both species A and B, is more pronounced than for $D_B = 7 \cdot 10^{-10}$ cm^2/s.

S/N Aspects and Limitations at Low Excitation Intensities (<1 μW)

As seen from Figure 4, reducing the excitation intensities to low excitation intensities (<1 μW) is a possibility to keep the concentration depletion under control. How-

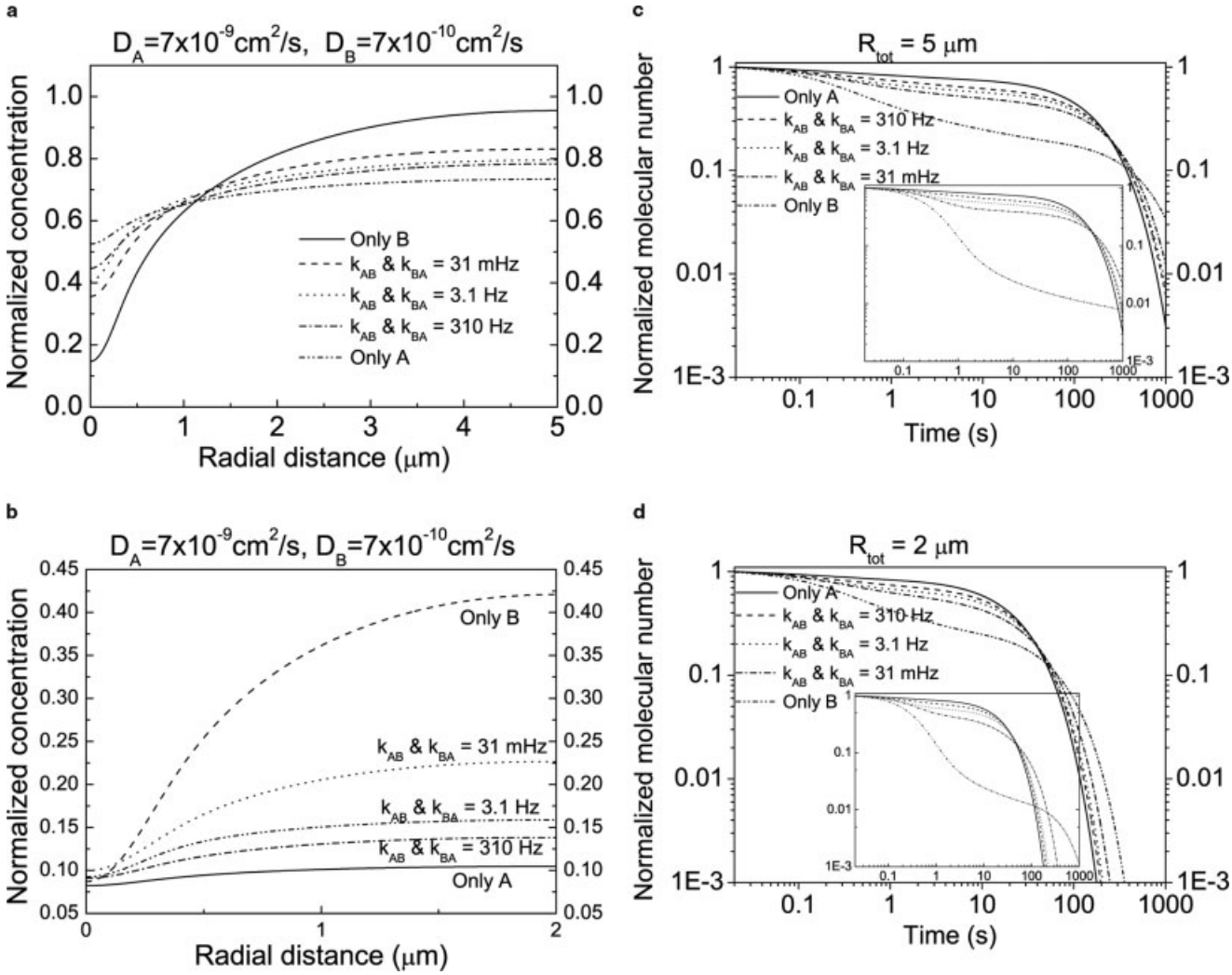

FIG. 5. (**a**) and (**b**) Calculated radial profiles of $c(r,t)$ for two species A and B, with diffusion coefficients $D_A = 7 \times 10^{-9}$ cm^2/s and $D_B = 7 \times 10^{-10}$ cm^2/s, as well as for species interconverting between states A and B at different rates of interconversion $k_{IC} = k_{AB} + k_{BA}$ (Eqs. (15) and (16)) and assuming $k_{AB} = k_{BA}$. (a) $P = 10$ μW, $R_{tot} = 5$ μm, $t = 60$ s (b) $P = 10$ μW, $R_{tot} = 2$ μm. $t = 60$ s (**c**) and (**d**) Mean fraction of molecules in the detection volume that has survived photobleaching, $\bar{N}(t)$, versus measurement/exposure time, for the same species and conditions as in Figures A and B, respectively. Insets: $\bar{N}(t)$ versus measurement/exposure time, with D_B ten times lower ($7 \cdot 10^{-11}$ cm^2/s).

ever, this also reduces the fluorescence emission rate per molecule, F_M, which is a major figure-of-merit for FCS measurements and which scales linearly with the excitation intensity at intensities well below saturation. At low F_M, where the product of F_M and the sampling time is far less than unity, the signal-to-noise ratio in FCS measurements can be estimated as (9)

$$S/N \propto F_M \, {t_{meas}}^{1/2} \tag{17}$$

To compensate for a reduction in S/N following from a lowered excitation intensity and F_M, thus requires a much longer total measurement time, t_{meas}, leading to an overall larger excitation energy exposure. For example, a reduction in excitation power from 2 to 1 μW in an FCS measurement would require a four times longer measurement time to compensate for the loss in S/N, leading to an overall doubled excitation energy on the sample. Moreover, with reduced excitation intensities, F_M may approach the dark count level of the detector(s). Given the parameters of TMR ($\sigma = 1.1 \times 10^{-16}$ cm^2, $k_{10} = 435 \times 10^6$ s^{-1}, $\Phi_F = 0.3$, $\Phi_{Fd} = 0.02$, excitation wavelength $\lambda_{exc} = 515$ nm), and assuming an excitation intensity of $I_{exc} = 1$ μW/($\pi\omega_0^2$), with $\omega_0 = 0.3$ μm, F_M would be ~600 cps/molecule. This is close to the typical dark count rate levels of avalanche photodiodes used in FCS measurements. The amplitude of the normalized correlation function in the presence of background can be expressed by (9)

$$G(0) - 1 = \frac{N}{(N + N_B)^2} \tag{18}$$

where N is the number of molecules in the detection volume, and $N_B = F_B/F_M$, with F_B denoting the background intensity. When N is in the same range as N_B, for instance due to a low F_M and/or a low concentration of

molecules, the amplitude of the correlation function, $G(0)$-1, will be significantly lower than $1/N$, incorrectly indicating a higher concentration of molecules than is actually present. A possible remedy for the dark count contribution to N_B can possibly be offered by modulation of the laser excitation, in combination with locked-in detection, as proposed for instance in confocal microscopy, mainly with the purpose to reduce cross-talk between several fluorophores (54). Pulsed excitation and laser-synchronized gating of the detection has been used to reduce background in single molecule fluorescence measurements (55), and similar hard-ware (56) as well as soft-ware (57) based detection gating has also been introduced in FCS measurements. However, while this gating reduces the laser light scattering contribution to the background, detector gating during excitation-free periods would limit the dark count contribution.

Concluding Remarks

In FCS cell surface measurements, photobleaching can be expected to be the by far most important photophysical limitation of the detected fluorescence intensity. It is found that the absence of apparently shorter measured passage times, such that the absolute majority of fluorescent molecules pass the detection volume without photobleaching, is clearly insufficient as a criterion to avoid photobleaching effects in FCS cellular studies. For the case that several species with different diffusion constants are studied within the same FCS measurement, a likely scenario is that fast diffusing species are less depleted in the volume of excitation than the slower fraction(s). However, also the inverse situation can occur for some combinations of experimental parameters common for a FCS measurement, i.e. slow fraction(s) can dominate over faster moving fractions due to less severe overall concentration depletion within the area of free diffusion. Taking also S/N aspects into account indicates that both the two main parameters measured—the concentration of molecules and the diffusive speed—can significantly decrease and increase as an effect of the excitation conditions. If several species or a distribution of species are to be measured on a cell surface by FCS, a proper range of excitation intensities or measurement times can be difficult to define, if the span of diffusive speeds, or concentrations among the species is too broad. As our calculations indicate, the resulting depletion effects also strongly depend on possible interchange between the species and the rates with which this interchange takes place. Well-defined measurement conditions, particularly in terms of excitation intensities and exposure times (including not only the time of FCS-recording), are required to be able to ascertain that distortions are minor, or to properly be able to correct for them. Without this knowledge, it is in general difficult to unambiguously state densities and mobilities of molecules on a cell surface from FCS measurements.

The outcome of these calculations is also relevant for intracellular measurements. A similar excitation procedure as used here would generate photobleaching along the whole propagation path of the beam through the cell. This has been investigated in detail by Delon et al., taking the relatively photolabile dye fluorescein isothiocyanate as a reference dye (45). A possible reduction of photobleaching depletion in intracellular measurements is offered by 2-photon excitation (TPE), where the volume of excitation can be reduced to comprise only the focus of the laser beam (58). Therefore, although Φ_D itself has been found to be higher for many dyes under TPE (59), the overall concentration depletion effects in intracellular FCS studies based on TPE (24,60) can often still be expected to be less severe than in cell surface studies. In their work, Delon et al. introduce a photobleaching parameter, $p_B = (\sigma\Phi_D P\lambda_{exc})/(bcD)$, where $P = I_0\pi{\omega_0}^2$ is the excitation power, b is Planck's constant, and c is the velocity of light. p_B is related to the probability of photobleaching per average molecular passage time through the laser beam. While for most situations discussed in the paper of Delon et al. $p_B < 1$, p_B was much higher under the conditions discussed here. Only for very fast membrane diffusion, combined with low excitation powers, we get a very low value of p_B (for instance, $p_B = 0.02$ for $D = 7 \times 10^{-8}$ cm^2/s and $P = 2.5$ μW, and $p_B = 0.8$ for $D = 7 \times 10^{-9}$ cm^2/s and $P = 10$ μW).

If proper experimental conditions are not possible to define, for which concentration depletion is tolerable and for which S/N is not strongly compromised, the outcome of this study suggests the use of additional measurement and data processing schemes. This would facilitate correction for depletion effects, but would at the same time also offer the possibility to extract additional information. To major processes influencing the depletion behavior belong diffusive properties, rate of possible interchange between states with different diffusive behavior, and the total area of free diffusion. Schemes to extract this information can for instance include series of FCS measurements with different excitation intensities and measurement times, where cumulative concentration depletion effects are continuously monitored, via the total fluorescence intensity, as well as by the development over time of decay times and amplitudes of the different FCS curves. An approach using the measured decay in fluorescence after start of excitation has earlier been introduced under the name continuous fluorescence microphotolysis (CFM) (61). A combined use of CFM and FCS has recently been used to analyze intracellular binding (62). In this context, presence of significant photobleaching makes it possible to determine the size of the areas within which the molecules under study are free to diffuse. By extrapolation of the fluorescence intensity decay to onset of excitation at $t = 0$, the initial concentration of molecules before photobleaching can be estimated. In general, molecules on cell surfaces often display heterogeneous properties in terms of diffusive speeds, densities, possible rates of interchange, and areas of free diffusion. This study demonstrates that the extent of concentration depletion depends strongly on these parameters, and can be quite different from one molecular species to another for a certain set of measurement parameters. Varying the measurement parameters within a series of measurements would then allow

a degree of species-selective analysis, changing the selectivity if needed from one measurement to the next within the whole set of measurements. In this sense, the outcome of the calculations provide keys for how to characterize these heterogeneities, and for how to extract more information from them than if the overall limitations would not exist.

APPENDIX

On a discrete form, with $c(r,t)$ approximated as an array $c_{i,j}$, where $r = i\,dr$ and $t = j\,dt$, Eq. (2) can be written

$$\frac{c_{i,j+1} - c_{i,j}}{dt} = \frac{1}{2}[\mathrm{A}c_{i,j+1} + \mathrm{A}c_{i,j}] \tag{A1}$$

The matrix A is given by

$$\mathrm{A}c_{0,j} = D\left[\frac{-2c_{0,j}}{h^2}\right] - k_i \times c_{0,j}$$

$$\mathrm{A}c_{i,j} = D\left[\frac{c_{i+1,j} - 2c_{i,j} + c_{i-1,j}}{h^2} + \frac{1}{i \times dr}\frac{c_{i+1,j} - c_{i-1,j}}{2\,dr}\right] - k_i\,c_{i,j} \quad \text{for } i \in (1, N-2) \tag{A2}$$

$$\mathrm{A}c_{N-1,j} = D\left[\frac{2c_{N-1,j}}{h^2}\right] - k_i\,c_{i,j}$$

Here, N is the number of discrete spatial steps, and the boundary condition of Eq. (4) has been applied

$$\frac{c_{i+1,j} - c_{i-1,j}}{dr} = 0 \quad \text{for } i = 0,\ N-1 \tag{A3}$$

which yields $c_{-1,j} = c_{1,j}$ and $c_N = c_{N-2}$. Eq. (A1) can be rearranged as

$$\mathrm{A}_1 c_{i,j+1} = \mathrm{A}_2 c_{i,j}, \text{corresponding to} \left[\frac{I}{dt} - \frac{\mathrm{A}}{2}\right] c_{i,j+1} = \left[\frac{I}{dt} + \frac{\mathrm{A}}{2}\right] c_{i,j} \tag{A4}$$

I is the unity matrix, and A is given by Eq. (A2). Given the initial condition of Eq. (3) on discrete form

$$c_{i0} = 1\ \forall i \tag{A5}$$

The array $c_{i,j}$ can be calculated for $i \in (0, N-1)$ and $j \in (0, K-1)$, where K is the number of steps in the time domain, as follows:

A: Calculate $b_j = \mathrm{A}_1 c_{i,j}$.
B: Calculate $c_{i,j+1}$ from $\mathrm{A}_2 c_{i,j+1} = b_j$ by Gauss elimination, backwards substitution, and iterative improvement.
C: Increase j with one step and repeat the procedure from A.

LITERATURE CITED

1. Madge D, Elson EL, Webb WW. Thermodynamic fluctuations in a reacting system-measurement by fluorescence correlation spectroscopy. Phys Rev Lett 1972;29:705–711.
2. Elson EL, Magde D. Fluorescence correlation spectroscopy. 1. Conceptual basis and theory. Biopolymers 1974;13:1–27.
3. Magde D, Elson EL, Webb WW. Fluorescence correlation spectroscopy. 2. An experimental realization. Biopolymers 1974;13:29–61.
4. Widengren J, Mets Ü. Conceptual basis of fluorescence correlation spectroscopy and related techniques as tools in bioscience. In: Zander C, Enderlein J, Keller RA, editors. Single Molecule Detection in Solution. Berlin: Wiley-VCH; 2002. p 69–120.
5. Krichevsky O, Bonnet G. Fluorescence correlation spectroscopy: the technique and its applications. Rep Prog Phys 2002;65:251–297.
6. Thompson NL, Lieto AM, Allen NW. Recent advances in fluorescence correlation spectroscopy. Curr Opin Struct Biol 2002;12:634–641.
7. Hess ST, Huang S, Heikal AA, Webb WW. Biological and chemical applications of fluorescence correlation spectroscopy: a review. Biochemistry 2002;41:697–705.
8. Haustein E, Schwille P. Ultrasensitive investigations of biological systems by fluorescence correlation spectroscopy. Methods 2003;29:153–166.
9. Koppel DE. Statistical accuracy in fluorescence correlation spectroscopy. Phys Rev A: Gen Phys 1974;10A:1938–1945.
10. Qian H. On the statistics of fluorescence correlation spectroscopy. Biophys Chem 1990;30:49–57.
11. Rigler R, Widengren J. Ultrasensitive detection of single molecules by fluorescence correlation spectroscopy. In: Klinge B, Owman C, editors. Bioscience. Sweden: Lund University Press; 1990. p 180–183.
12. Rigler R, Mets Ü, Widengren J, Kask P. Fluorescence correlation spectroscopy with high count rate and low background: analysis of translational diffusion. Eur Biophys J 1993;22:169–175.
13. Widengren J, Rigler R. Mechanisms of photobleaching investigated by fluorescence correlation spectroscopy. Bioimaging 1996;4:149–157.
14. Eggeling C, Widengren J, Rigler R, Seidel C. Photobleaching of fluorescent dyes under conditions used for single-molecule-detection: evidence of two-step photolysis. Anal Chem 1998;70:2651–2659.
15. Elson EL. Fluorescence correlation spectroscopy measures molecular transport in cells. Traffic 2001;2:789–796.
16. Verkman AS. Solute and macromolecular diffusion in cellular aqueous compartments. Trends Biochem Sci 2002;27:27–33.
17. Phair RD, Mistelli T. Kinetic modelling approaches to in vivo imaging. Nat Rev Mol Cell Biol 2001;2:898–907.
18. Rigler R. Fluorescence correlations, single molecule detection and large number screening. Applications in biotechnology. J Biotechnol 1995;41:177–186.
19. Widengren J, Rigler R. Fluorescence correlation spectroscopy as a tool to investigate chemical reactions in solutions and on cell surfaces. Cell Mol Biol 1998;44:857–879.
20. Brock R, Hink MA, Jovin TM. Fluorescence correlation spectroscopy of cells in the presence of autofluorescence. Biophys J 1998;75:2547–2557.
21. Politz JC, Browne ES, Wolf DE, Pederson T. Intranuclear dissusion and hybridization of oligonucleotides measured by fluorescence correlation spectrosocopy in living cells. Proc Natl Acad Sci USA 1998;95:6043–6048.
22. Brock R, Va'mosi G, Vereb G, Jovin TM. Rapid characterization of green fluorescent protein fusion proteins on the molecular and cellular level by fluorescence correlation microscopy. Proc Natl Acad Sci USA 1999;96:10123–10128.
23. Rigler R, Pramanik A, Jonasson P, Kratz G, Jansson OT, Nygren PÅ, Ståhl S, Ekberg K, Johansson BL, Uhle'n S, Uhle'n M, Jörnvall H, Wahren J. Specific binding of proinsulin C-peptide to human cell membranes. Proc Natl Acad Sci USA 1999;96:13318–13323.
24. Schwille P, Haupts U, Maiti S, Webb WW. Molecular dynamics in living cells observed by fluorescence correlation spectrosocpy with one- and two-photon excitation. Biophys J 1999;77:2251–2265.
25. Schwille P, Korlach J, Webb WW. Fluorescence Correlation Spectroscopy with single-molecule sensitivity on cell and model membranes. Cytometry 1999;36:176–182.
26. Pramanik A, Rigler R. Ligand-receptor interactions in the membrane of cultured cells monitored by fluorescence correlation spectroscopy. Biol Chem 2001;382:371–378.
27. Pramanik A, Ekberg K, Zhong Z, Shafqat J, Henriksson M, Jansson O, Tibell A, Tally M, Wahren J, Jörnvall H, Rigler R, Johansson J. C-peptide binding to human cell membranes: importance of Glu27. Biochem Biophys Res Commun 1998;284:94–98.
28. Yoshida N, Kinjo M, Tamura M. Microenvironment of endosomal aqueous phase investigated by the mobility of microparticles using fluorescence correlation spectroscopy. Biochem Biophys Res Commun 2001;280:312–318.
29. Brock R, Jovin TM. Fluorescence Correlation Microscopy (FCM): fluorescence correlation spectroscopy (FCS) in cell biology. In: Rigler R,

Elson EL, editors. Fluorescence Correlation Spectroscopy. Theory and Applications. Heidelberg: Springer-Verlag; 2002. p 132–161.
30. Muto T, Saito K, Tamura M, Kinjo M. Microenvironment analysis in squid axons using fluorescence correlation spectroscopy and laser scanning microscopy. Acta Histochem Cytochem 2002;35: 87–91.
31. Pramanik A, Rigler R. FCS-analysis of ligand-receptor interactions in living cells. In: Rigler R, Elson EL, editors. Fluorescence Correlation Spectroscopy. Theory and Applications. Heidelberg: Springer-Verlag; 2002. p 101–131.
32. Takahashi Y, Bark N, Kinjo M, Rigler R. Fluorescence correlation spectroscopy (FCS) analysis of human red blood cell system. Opt Rev 2003;10:596–599.
33. Waizenegger T, Fischer R, Brock R. Intracellular concentration measurements in adherent cells: a comparison of import efficiencies of cell-permeable peptides. Biol Chem 2002;383:291–299.
34. Bacia K, Scherfeld D, Kahya N, Schwille P. Fluorescence correlation spectroscopy relates rafts in model and native membranes. Biophys J 2004;87:1034–1043.
35. Briddon SJ, Middleton RJ, Cordeaux Y, Flavin FM, Weinstein JA, George MW, Kellam B, Hill SJ. Quantitative analysis of the formation and diffusion of A_1-adenosine receptor-antagonist complexes in single living cells. Proc Natl Acad Sci USA 2004;101:4673–4678.
36. Saito K, Wada I, Tamura M, Kinjo M. Direct detection of caspase-3 activation in single live cells by cross-correlation analysis. Biochem Biophys Res Commun 2004;324:849–854.
37. Wachsmut M, Waldeck W, Langowski J. Anomalous diffusion of fluorescent probes inside living cell nuclei investigated by spatially-resolved fluorescence correlation spectroscopy. J Mol Biol 2000;298: 677–689.
38. Gennerich A, Schild D. Fluorescence correlation spectroscopy in small cytosolic compartments depends critically on the diffusion model used. Biophys J 2000;79:3294–3306.
39. Gennerich A, Schild D. Anisotropic diffusion in mitral cell dendrites revealed by fluorescence correlation spectroscopy. Biophys J 2002;83: 510–522.
40. Dittrich P, Malvezzi-Campeggi F, Jahnz M, Schwille P. Accessing molecular dynamics in cells by fluorescence correlation spectroscopy. Biol Chem 2001;382:491–494.
41. Fradin C, Asmahan A-A, Granek R, Elbaum M. Fluorescence correlation spectroscopy close to a fluctuating membrane. Biophys J 2003; 84:2005–2020.
42. Milon S, Hovius R, Vogel H, Wohland T. Factors influencing fluorescence correlation spectroscopy measurements on membranes: simulations and experiments. Chem Phys 2003;288:171–186.
43. Weiss M, Hashimoto H, Nilsson T. Anomalous protein diffusion in living cells as seen by fluorescence correlation spectroscopy. Biophys J 2003;84:4043–4052.
44. Burden DL, Kasianowicz JJ. Diffusion bias and photophysical dynamics of single molecules in unsupported lipid bilayer membranes probed by confocal microscopy. J Phys Chem B 2000;104:6103–6107.
45. Delon A, Usson Y, Derouard J, Biben T, Souchier. Photobleaching, mobility, and compartmentalization: inferences in fluorescence correlation spectroscopy. J Fluoresc 2004;14:255–267.
46. Widengren J, Mets Ü, Rigler R. Fluorescence correlation spectroscopy of triplet states in solution: a theoretical and experimental study. J Phys Chem 1995;99:13368–13379.
47. Press WH, Flannery BP, Teukolsky SA, Vetterling WT. Numerical Recipes. Cambridge: Cambridge University Press; 1986.
48. Eggeling C. Ph.D. Thesis, Göttingen University, 1999.
49. Hillman GM, Schlessinger J. Lateral diffusion of epidermal growth factor complexed to its surface receptors does not account for the thermal sensitivity of patch formation and endocytosis. Biochemistry 1982;21:1667–1672.
50. Schütz GJ, Schindler H, Schmidt T. Imaging of single molecule diffusion. Proc Natl Acad Sci USA 1996;93:2926–2929.
51. Widengren J. Photophysical aspects of fluorescence correlation spectroscopy measurements. In: Rigler R, Elson EL, editors. Fluorescence Correlation Spectroscopy—Theory and Applications. Heidelberg: Springer Verlag; 2002. pp. 276–300.
52. Cherry RJ, Smith PR, Morrison IEG, Fernandez N. Mobility of cell surface receptors: a re-evaluation. FEBS Lett 1998;430:88–91.
53. Lippincott-Schwartz J, Snapp E, Kenworthy A. Studying protein dynamics in living cells. Nat Rev Cell Mol Biol 2001;2:444–456.
54. Carlsson K, Åslund N, Mossberg K, Philip J. Simultaneous confocal recording of multiple fluorescent labels with improved channel separation. J Microsc 1994;176:287–299.
55. Shera EB, Seitzinger NK, Davis LM, Keller RA, Soper SA. Detection of single fluorescent molecules. Chem Phys Lett 1990;174:553–557.
56. Lamb DC, Schenk A, Rocker C, Scalpi-Happ C, Nienhaus GU. Sensitivity enhancement in fluorescence correlation spectroscopy of multiple species using time-gated detection. Biophys J 2000;79:1129–1138.
57. Eggeling C, Berger S, Brand L, Fries JR, Schaffer J, Volkmer A, Seidel CAM. Data registration and selective single-molecule analysis using multi-parameter fluorescence detection. J Biotechol 2001;86:163–180.
58. Denk W, Strickler JH, Webb WW. Two-photon laser scanning microscopy. Science 1990;248:73.
59. Sanchez EJ, Novotny L, Holtom GR, Xie XS. Room-temperature fluorescence imaging and spectroscopy of single molecules by two-photon excitation. J Phys Chem 1997;101:7019–7023.
60. Berland KM, So PT, Gratton E. Two-photon fluorescence correlations spectroscopy: method and application to the intracellular environment. Biophys J 1995;68:694–701.
61. Brunger A, Peters R, Schulten K. Continuous fluorescence microphotolysis to observe lateral diffusion in membranes. Theoretical methods and applications. J Chem Phys 1985;82:2147–2160.
62. Wachsmuth M, Weidemann T, Mueller G, Hoffmann-Rohrer UW, Knoch TA, Waldeck W, Langowski J. Analyzing intracellular binding and diffusion with continuous fluorescence photobleaching. Biophys J 2003;84:3353–3363.